Angular decay coefficients of J/ψ mesons at forward rapidity from p+p collisions at √s=510 GeV

(PHENIX Collaboration) Adare, A.; ...; Dumancic, Mirta; ...; Makek, Mihael; ...; Vukman, Nikola; ...; Zou, L.

Angular decay coefficients of J/ψ mesons at forward rapidity from $p+p$ collisions at $\sqrt{s}=510$ GeV

A. Adare,[12] C. Aidala,[41] N. N. Ajitanand,[58,*] Y. Akiba,[53,54,†] R. Akimoto,[11] M. Alfred,[23] V. Andrieux,[41] K. Aoki,[31,53] N. Apadula,[28,59] Y. Aramaki,[53] H. Asano,[34,53] E. T. Atomssa,[59] T. C. Awes,[49] C. Ayuso,[41] B. Azmoun,[7] V. Babintsev,[24] M. Bai,[6] N. S. Bandara,[40] B. Bannier,[59] K. N. Barish,[8] S. Bathe,[5,54] A. Bazilevsky,[7] M. Beaumier,[8] S. Beckman,[12] R. Belmont,[12,41] A. Berdnikov,[56] Y. Berdnikov,[56] D. Black,[8] D. S. Blau,[33] M. Boer,[37] J. S. Bok,[47] E. K. Bownes,[42] K. Boyle,[54] M. L. Brooks,[37] J. Bryslawskyj,[5,8] H. Buesching,[7] V. Bumazhnov,[24] C. Butler,[20] S. Campbell,[13,28] V. Canoa Roman,[59] R. Cervantes,[59] C.-H. Chen,[54] C. Y. Chi,[13] M. Chiu,[7] I. J. Choi,[25] J. B. Choi,[10,*] T. Chujo,[62] Z. Citron,[64] M. Connors,[20,54] N. Cronin,[42,59] M. Csanád,[16] T. Csörgő,[17,65] T. W. Danley,[48] A. Datta,[46] M. S. Daugherity,[1] G. David,[7] K. DeBlasio,[46] K. Dehmelt,[59] A. Denisov,[24] A. Deshpande,[54,59] E. J. Desmond,[7] L. Ding,[28] A. Dion,[59] D. Dixit,[59] J. H. Do,[66] A. Drees,[59] K. A. Drees,[6] M. Dumancic,[64] J. M. Durham,[37] A. Durum,[24] J. P. Dusing,[42] T. Elder,[20] A. Enokizono,[53,55] H. En'yo,[53] S. Esumi,[62] B. Fadem,[42] W. Fan,[59] N. Feege,[59] D. E. Fields,[46] M. Finger,[9] M. Finger, Jr.,[9] S. L. Fokin,[33] J. E. Frantz,[48] A. Franz,[7] A. D. Frawley,[19] Y. Fukuda,[62] C. Gal,[59] P. Gallus,[14] P. Garg,[3,59] H. Ge,[59] F. Giordano,[25] A. Glenn,[36] Y. Goto,[53,54] N. Grau,[2] S. V. Greene,[63] M. Grosse Perdekamp,[25] Y. Gu,[58] T. Gunji,[11] H. Guragain,[20] T. Hachiya,[53,54] J. S. Haggerty,[7] K. I. Hahn,[18] H. Hamagaki,[11] H. F. Hamilton,[1] S. Y. Han,[18] J. Hanks,[59] S. Hasegawa,[29] T. O. S. Haseler,[20] X. He,[20] T. K. Hemmick,[59] J. C. Hill,[28] K. Hill,[12] R. S. Hollis,[8] K. Homma,[22] B. Hong,[32] T. Hoshino,[22] N. Hotvedt,[28] J. Huang,[7,37] S. Huang,[63] Y. Ikeda,[53] K. Imai,[29] Y. Imazu,[53] J. Imrek,[15] M. Inaba,[62] A. Iordanova,[8] D. Isenhower,[1] Y. Ito,[44] D. Ivanishchev,[52] B. V. Jacak,[59] S. J. Jeon,[43] M. Jezghani,[20] Z. Ji,[59] J. Jia,[7,58] X. Jiang,[37] B. M. Johnson,[7,20] E. Joo,[32] K. S. Joo,[43] V. Jorjadze,[59] D. Jouan,[50] D. S. Jumper,[25] J. H. Kang,[66] J. S. Kang,[21] D. Kapukchyan,[8] S. Karthas,[59] D. Kawall,[40] A. V. Kazantsev,[33] T. Kempel,[28] J. A. Key,[46] V. Khachatryan,[59] A. Khanzadeev,[52] K. Kihara,[62] C. Kim,[8,32] D. H. Kim,[18] D. J. Kim,[30] E.-J. Kim,[10] H.-J. Kim,[66] M. Kim,[57] M. H. Kim,[32] Y. K. Kim,[21] M. L. Kimball,[1] D. Kincses,[16] E. Kistenev,[7] J. Klatsky,[19] D. Kleinjan,[8] P. Kline,[59] T. Koblesky,[12] M. Kofarago,[16,65] J. Koster,[54] J. R. Kotler,[42] D. Kotov,[52,56] S. Kudo,[62] K. Kurita,[55] M. Kurosawa,[53,54] Y. Kwon,[66] R. Lacey,[58] J. G. Lajoie,[28] E. O. Lallow,[42] A. Lebedev,[28] K. B. Lee,[37] S. Lee,[66] S. H. Lee,[59] M. J. Leitch,[37] M. Leitgab,[25] Y. H. Leung,[59] N. A. Lewis,[41] X. Li,[37] S. H. Lim,[37,66] L. D. Liu,[51] M. X. Liu,[37] V-R Loggins,[25] V.-R. Loggins,[25] K. Lovasz,[15] D. Lynch,[7] T. Majoros,[15] Y. I. Makdisi,[6] M. Makek,[64,67] M. Malaev,[52] A. Manion,[59] V. I. Manko,[33] E. Mannel,[7] H. Masuda,[55] M. McCumber,[37] P. L. McGaughey,[37] D. McGlinchey,[12] C. McKinney,[25] A. Meles,[47] A. R. Mendez,[42] M. Mendoza,[8] B. Meredith,[13] Y. Miake,[62] A. C. Mignerey,[39] D. E. Mihalik,[59] A. J. Miller,[1] A. Milov,[64] D. K. Mishra,[4] J. T. Mitchell,[7] G. Mitsuka,[54] S. Miyasaka,[53,61] S. Mizuno,[53,62] P. Montuenga,[25] T. Moon,[66] D. P. Morrison,[7] S. I. M. Morrow,[63] T. V. Moukhanova,[33] T. Murakami,[34,53] J. Murata,[53,55] A. Mwai,[58] K. Nagai,[61] S. Nagamiya,[31,53] K. Nagashima,[22] T. Nagashima,[55] J. L. Nagle,[12] M. I. Nagy,[16] I. Nakagawa,[53,54] H. Nakagomi,[53,62] K. Nakano,[53,61] C. Nattrass,[60] P. K. Netrakanti,[4] M. Nihashi,[22,53] T. Niida,[62] R. Nouicer,[7,54] T. Novák,[17,65] N. Novitzky,[30,59] R. Novotny,[14] A. S. Nyanin,[33] E. O'Brien,[7] C. A. Ogilvie,[28] J. D. Orjuela Koop,[12] J. D. Osborn,[41] A. Oskarsson,[38] G. J. Ottino,[46] K. Ozawa,[31,62] R. Pak,[7] V. Pantuev,[26] V. Papavassiliou,[47] J. S. Park,[57] S. Park,[53,57,59] S. F. Pate,[47] L. Patel,[20] M. Patel,[28] J.-C. Peng,[25] W. Peng,[63] D. V. Perepelitsa,[7,12,13] G. D. N. Perera,[47] D. Yu. Peressounko,[33] C. E. PerezLara,[59] J. Perry,[28] R. Petti,[7,59] M. Phipps,[7,25] C. Pinkenburg,[7] R. Pinson,[1] R. P. Pisani,[7] C. J. Press,[42] A. Pun,[48] M. L. Purschke,[7] J. Rak,[30] I. Ravinovich,[64] K. F. Read,[49,60] D. Reynolds,[58] V. Riabov,[45,52] Y. Riabov,[52,56] D. Richford,[5] T. Rinn,[28] N. Riveli,[48] D. Roach,[63] S. D. Rolnick,[8] M. Rosati,[28] Z. Rowan,[5] J. G. Rubin,[41] J. Runchey,[28] A. S. Safonov,[56] N. Saito,[31] T. Sakaguchi,[7] H. Sako,[29] V. Samsonov,[45,52] M. Sarsour,[20] K. Sato,[62] S. Sato,[29] S. Sawada,[31] B. Schaefer,[63] B. K. Schmoll,[60] K. Sedgwick,[8] J. Seele,[54] R. Seidl,[53,54] A. Sen,[28,60] R. Seto,[8] P. Sett,[4] A. Sexton,[39] D. Sharma,[59] I. Shein,[24] T.-A. Shibata,[53,61] K. Shigaki,[22] M. Shimomura,[28,44] T. Shioya,[62] P. Shukla,[4] A. Sickles,[7,25] C. L. Silva,[37] J. A. Silva,[42] D. Silvermyr,[38,49] B. K. Singh,[3] C. P. Singh,[3] V. Singh,[3] M. Slunečka,[9] K. L. Smith,[19] M. Snowball,[37] R. A. Soltz,[36] W. E. Sondheim,[37] S. P. Sorensen,[60] I. V. Sourikova,[7] P. W. Stankus,[49] M. Stepanov,[40,*] H. Stien,[1] S. P. Stoll,[7] T. Sugitate,[22] A. Sukhanov,[7] T. Sumita,[53] J. Sun,[59] S. Syed,[20] J. Sziklai,[65] A. Takahara,[11] A. Takeda,[44] A. Taketani,[53,54] K. Tanida,[29,54,57] M. J. Tannenbaum,[7] S. Tarafdar,[63,64] A. Taranenko,[45,58] G. Tarnai,[15] R. Tieulent,[20] A. Timilsina,[28] T. Todoroki,[53,62] M. Tomášek,[14] H. Torii,[11] C. L. Towell,[1] M. Towell,[1] R. Towell,[1] R. S. Towell,[1] I. Tserruya,[64] Y. Ueda,[22] B. Ujvari,[15] H. W. van Hecke,[37] M. Vargyas,[16,65] S. Vazquez-Carson,[12] J. Velkovska,[63] M. Virius,[14] V. Vrba,[14,27] N. Vukman,[67] E. Vznuzdaev,[52] X. R. Wang,[47,54] Z. Wang,[5] D. Watanabe,[22] Y. Watanabe,[53,54] Y. S. Watanabe,[11,31] F. Wei,[47] S. Whitaker,[28] S. Wolin,[25] C. P. Wong,[20] C. L. Woody,[7] M. Wysocki,[49] B. Xia,[48] C. Xu,[47] Q. Xu,[63] L. Xue,[20] S. Yalcin,[59] Y. L. Yamaguchi,[11,54,59] H. Yamamoto,[62] A. Yanovich,[24] P. Yin,[12] J. H. Yoo,[32] I. Yoon,[57] I. Younus,[35] H. Yu,[47,51] I. E. Yushmanov,[33] W. A. Zajc,[13] A. Zelenski,[6] S. Zharko,[56] and L. Zou[8]

(PHENIX Collaboration)

[1]*Abilene Christian University, Abilene, Texas 79699, USA*
[2]*Department of Physics, Augustana University, Sioux Falls, South Dakota 57197, USA*

[3]*Department of Physics, Banaras Hindu University, Varanasi 221005, India*
[4]*Bhabha Atomic Research Centre, Bombay 400 085, India*
[5]*Baruch College, City University of New York, New York, New York 10010 USA*
[6]*Collider-Accelerator Department, Brookhaven National Laboratory, Upton, New York 11973-5000, USA*
[7]*Physics Department, Brookhaven National Laboratory, Upton, New York 11973-5000, USA*
[8]*University of California-Riverside, Riverside, California 92521, USA*
[9]*Charles University, Ovocný trh 5, Praha 1, 116 36 Prague, Czech Republic*
[10]*Chonbuk National University, Jeonju 561-756, Korea*
[11]*Center for Nuclear Study, Graduate School of Science, University of Tokyo, 7-3-1 Hongo, Bunkyo, Tokyo 113-0033, Japan*
[12]*University of Colorado, Boulder, Colorado 80309, USA*
[13]*Columbia University, New York, New York 10027 and Nevis Laboratories, Irvington, New York 10533, USA*
[14]*Czech Technical University, Zikova 4, 166 36 Prague 6, Czech Republic*
[15]*Debrecen University, H-4010 Debrecen, Egyetem tér 1, Hungary*
[16]*ELTE, Eötvös Loránd University, H-1117 Budapest, Pázmány P. s. 1/A, Hungary*
[17]*Eszterházy Károly University, Károly Róbert Campus, H-3200 Gyöngyös, Mátrai út 36, Hungary*
[18]*Ewha Womans University, Seoul 120-750, Korea*
[19]*Florida State University, Tallahassee, Florida 32306, USA*
[20]*Georgia State University, Atlanta, Georgia 30303, USA*
[21]*Hanyang University, Seoul 133-792, Korea*
[22]*Hiroshima University, Kagamiyama, Higashi-Hiroshima 739-8526, Japan*
[23]*Department of Physics and Astronomy, Howard University, Washington DC 20059, USA*
[24]*IHEP Protvino, State Research Center of Russian Federation, Institute for High Energy Physics, Protvino 142281, Russia*
[25]*University of Illinois at Urbana-Champaign, Urbana, Illinois 61801, USA*
[26]*Institute for Nuclear Research of the Russian Academy of Sciences, prospekt 60-letiya Oktyabrya 7a, Moscow 117312, Russia*
[27]*Institute of Physics, Academy of Sciences of the Czech Republic, Na Slovance 2, 182 21 Prague 8, Czech Republic*
[28]*Iowa State University, Ames, Iowa 50011, USA*
[29]*Advanced Science Research Center, Japan Atomic Energy Agency, 2-4 Shirakata Shirane, Tokai-mura, Naka-gun, Ibaraki-ken 319-1195, Japan*
[30]*Helsinki Institute of Physics and University of Jyväskylä, P.O.Box 35, FI-40014 Jyväskylä, Finland*
[31]*KEK, High Energy Accelerator Research Organization, Tsukuba, Ibaraki 305-0801, Japan*
[32]*Korea University, Seoul 136-701, Korea*
[33]*National Research Center "Kurchatov Institute", Moscow 123098, Russia*
[34]*Kyoto University, Kyoto 606-8502, Japan*
[35]*Physics Department, Lahore University of Management Sciences, Lahore 54792, Pakistan*
[36]*Lawrence Livermore National Laboratory, Livermore, California 94550, USA*
[37]*Los Alamos National Laboratory, Los Alamos, New Mexico 87545, USA*
[38]*Department of Physics, Lund University, Box 118, SE-221 00 Lund, Sweden*
[39]*University of Maryland, College Park, Maryland 20742, USA*
[40]*Department of Physics, University of Massachusetts, Amherst, Massachusetts 01003-9337, USA*
[41]*Department of Physics, University of Michigan, Ann Arbor, Michigan 48109-1040, USA*
[42]*Muhlenberg College, Allentown, Pennsylvania 18104-5586, USA*
[43]*Myongji University, Yongin, Kyonggido 449-728, Korea*
[44]*Nara Women's University, Kita-uoya Nishi-machi Nara 630-8506, Japan*
[45]*National Research Nuclear University, MEPhI, Moscow Engineering Physics Institute, Moscow 115409, Russia*
[46]*University of New Mexico, Albuquerque, New Mexico 87131, USA*
[47]*New Mexico State University, Las Cruces, New Mexico 88003, USA*
[48]*Department of Physics and Astronomy, Ohio University, Athens, Ohio 45701, USA*
[49]*Oak Ridge National Laboratory, Oak Ridge, Tennessee 37831, USA*
[50]*IPN-Orsay, Univ. Paris-Sud, CNRS/IN2P3, Université Paris-Saclay, BP1, F-91406 Orsay, France*
[51]*Peking University, Beijing 100871, People's Republic of China*
[52]*PNPI, Petersburg Nuclear Physics Institute, Gatchina, Leningrad region 188300, Russia*
[53]*RIKEN Nishina Center for Accelerator-Based Science, Wako, Saitama 351-0198, Japan*
[54]*RIKEN BNL Research Center, Brookhaven National Laboratory, Upton, New York 11973-5000, USA*
[55]*Physics Department, Rikkyo University, 3-34-1 Nishi-Ikebukuro, Toshima, Tokyo 171-8501, Japan*

[56]Saint Petersburg State Polytechnic University, St. Petersburg, 195251 Russia
[57]Department of Physics and Astronomy, Seoul National University, Seoul 151-742, Korea
[58]Chemistry Department, Stony Brook University, SUNY, Stony Brook, New York 11794-3400, USA
[59]Department of Physics and Astronomy, Stony Brook University, SUNY, Stony Brook, New York 11794-3800, USA
[60]University of Tennessee, Knoxville, Tennessee 37996, USA
[61]Department of Physics, Tokyo Institute of Technology, Oh-okayama, Meguro, Tokyo 152-8551, Japan
[62]Center for Integrated Research in Fundamental Science and Engineering, University of Tsukuba, Tsukuba, Ibaraki 305, Japan
[63]Vanderbilt University, Nashville, Tennessee 37235, USA
[64]Weizmann Institute, Rehovot 76100, Israel
[65]Institute for Particle and Nuclear Physics, Wigner Research Centre for Physics, Hungarian Academy of Sciences (Wigner RCP, RMKI) H-1525 Budapest 114, POBox 49, Budapest, Hungary
[66]Yonsei University, IPAP, Seoul 120-749, Korea
[67]Department of Physics, Faculty of Science, University of Zagreb, Bijenička 32, HR-10002 Zagreb, Croatia

(Received 21 December 2016; published 8 May 2017)

We report the first measurement of the full angular distribution for inclusive $J/\psi \to \mu^+\mu^-$ decays in $p+p$ collisions at $\sqrt{s} = 510$ GeV. The measurements are made for J/ψ transverse momentum $2 < p_T < 10$ GeV/c and rapidity $1.2 < y < 2.2$ in the Helicity, Collins-Soper, and Gottfried-Jackson reference frames. In all frames the polar coefficient λ_θ is strongly negative at low p_T and becomes close to zero at high p_T, while the azimuthal coefficient λ_ϕ is close to zero at low p_T, and becomes slightly negative at higher p_T. The frame-independent coefficient $\tilde{\lambda}$ is strongly negative at all p_T in all frames. The data are compared to the theoretical predictions provided by nonrelativistic quantum chromodynamics models.

DOI: 10.1103/PhysRevD.95.092003

I. INTRODUCTION

Measurements of heavy quark bound states provide a unique opportunity to explore basic quantum chromodynamics (QCD). Because the energy scale of the heavy quark mass is larger than the hadronization scale, nonrelativistic QCD (NRQCD) techniques can be applied to provide theoretical access to hadronization. Charmonium, the bound state of a charm and anticharm quark, is an especially convenient laboratory as it decays with a considerable branching fraction into two leptons. It is composed of two moderately heavy quarks, and is more copiously available than bottomonium (a bottom and antibottom bound state).

The charmonium wave function can be expressed as a combination of intermediate state contributions formed during the $c-\bar{c}$ hadronization stage. The S-wave charmonium wave function can be calculated from an expansion in a series of the charm and anticharm velocity ν in the charmonium rest frame [1],

$$|\psi_Q\rangle = \mathcal{O}(1)|^3S_1^{(1)}\rangle + \mathcal{O}(\nu)|^3P_J^{(8)}g\rangle + \mathcal{O}(\nu^2)|^3S_1^{(8)}gg\rangle + \mathcal{O}(\nu^2)|^3S_0^{(8)}g\rangle + \cdots, \quad (1)$$

in the spectroscopic notation $^{2S+1}L_J$. The series contains color singlet$^{(1)}$ and color octet$^{(8)}$ states. The nonrelativistic operators $\mathcal{O}$ are parametrized from experimental results.

Several models have been proposed for the production of J/ψ mesons, each one with a different interpretation of these intermediate states. The color evaporation model (CEM) [2], applied only to hadronic collisions, assumes that the nonrelativistic amplitude is constant from twice the charm quark mass to twice the D meson mass and zero elsewhere. All relativistic diagrams to a fixed order in α_s producing a charm and anticharm quark in the final state are included. The original color-singlet model (CSM) [3] explicitly requires the $c\bar{c}$ pair produced in the hard scattering to be on-shell and in the same quantum state as the hadronized J/ψ ($^{2S+1}L_J = {}^3S_1$). The nonrelativistic amplitude is taken as the real-space J/ψ wave function evaluated at the origin. Early calculations of the CSM at LO in α_s under-predicted cross sections at CDF [4] and PHENIX [5]. Recent calculations at next-to-leading order (NLO) [6,7] and next-to-next-to-leading order (NNLO) [8] increase the predicted cross section. NRQCD calculations [1] predict nonnegligible contributions from $c\bar{c}$ production in the color-octet configuration, leading to a larger cross section and better agreement with data than the current CSM calculations.

Several terms in Eq. (1) produce similar J/ψ cross sections and transverse momentum behavior, but can be

*Deceased
†akiba@rcf.rhic.bnl.gov

experimentally distinguished because of their different helicities. The angular distribution of spin $\frac{1}{2}$ lepton decays from a spin 1 quarkonium state is derived from the density matrix $\rho_{m'm}$ (where m' and m have the possible values–1,0,1) of the production process and parity conservation constraints [9–11].

The elements of the matrix are identified as

$$\begin{aligned} W_L &= \rho_{00} \qquad \text{(longitudinal helicity)} \\ W_T &= \rho_{11} - \rho_{-1-1} \qquad \text{(transverse helicity)} \\ W_\Delta &= \frac{1}{\sqrt{2}}(\rho_{10} + \rho_{01}) \qquad \text{(single spin-flip)} \\ W_{\Delta\Delta} &= \rho_{1-1} \qquad \text{(double spin-flip)} \end{aligned} \tag{2}$$

The angular distribution of the positive lepton from the J/ψ decay can be written as

$$\frac{dN}{d\cos\theta d\phi} \propto 1 + \lambda_\theta \cos^2\theta + \lambda_{\theta\phi} \sin 2\theta \cos\phi + \lambda_\phi \sin^2\theta \cos 2\phi \tag{3}$$

where,

$$\begin{aligned} \lambda_\theta &= \frac{W_T - W_L}{W_T + W_L} \\ \lambda_\phi &= \frac{2W_{\Delta\Delta}}{W_T + W_L} \\ \lambda_{\theta\phi} &= \frac{\sqrt{2}W_\Delta}{W_T + W_L} \end{aligned}$$

which we call the polar (λ_θ), the azimuthal (λ_ϕ) and the "mixed" ($\lambda_{\theta\phi}$) angular decay coefficients.

The angles ϕ and θ are measured relative to a reference frame defined such that the $\hat{x}$ and $\hat{z}$-axes lie in the production plane, formed by the momenta of the colliding protons and the particle produced. The direction of the $\hat{z}$-axis within the production plane is arbitrary. The simplest frame to study the particle wave function is the one in which the density matrix has only diagonal elements, or the single and double spin-flip terms are zero. This simplest frame is also called the natural frame and is identified when the azimuthal coefficients in (3) are zero. The three most common frames used in particle angular distribution studies are (Fig. 1):

The Helicity frame (HX) [9], traditionally used in collider experiments, takes the $\hat{z}$-axis as the spin-1 particle momentum direction.

The Collins-Soper frame (CS) [10], widely used in Drell-Yan measurements, chooses the $\hat{z}$-axis as the difference between the momenta of the colliding partons boosted into the spin-1 particle rest frame. Note that while the original paper [10] and subsequent theoretical studies used colliding parton momenta in their calculations, the colliding hadron momenta are used here, because we do not have information about the parton momenta.

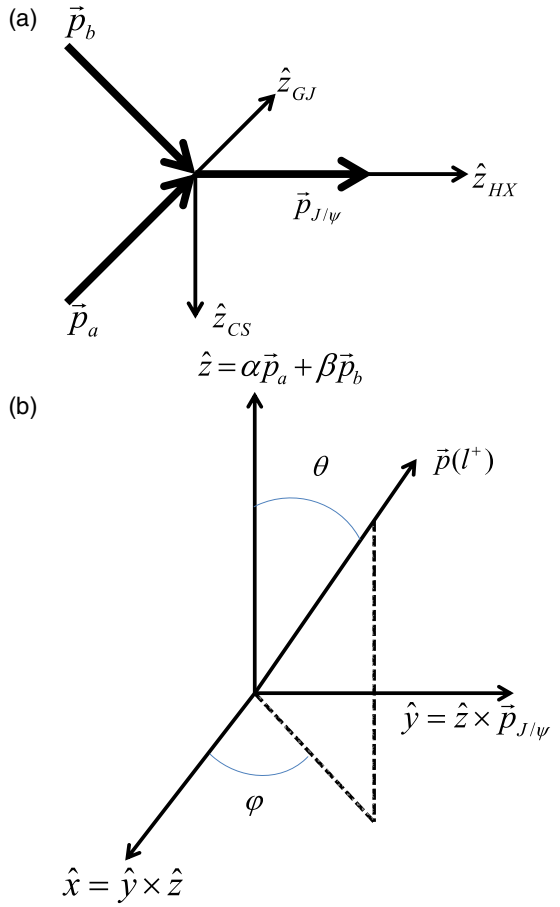

FIG. 1. Reference frames and coordinate system used in this analysis. The $\hat{x}$ and $\hat{z}$-axes are chosen to lie in the production plane determined by the colliding hadrons and the particle produced (a J/ψ in this figure). (a) shows the production plane and the direction convention for the $\hat{z}$ in the Collins-Soper (CS), Helicity (HX) and Gottfried-Jackson (GJ) reference frames. $\vec{p}_a$, $\vec{p}_b$ in this diagram, represent colliding parton momenta. Note that in an experiment we do not know parton momenta and use colliding hadron momenta instead. In (b) the angles θ and ϕ represent the direction of the positive decay lepton in the corresponding reference frame.

The Gottfried-Jackson frame (GJ) [11], typically used in fixed target experiments, takes the $\hat{z}$-axis as the beam momentum boosted into the spin-1 particle rest frame. At forward angles in a collider environment, the definition of the GJ frame depends heavily on which beam is used in the definition. If the beam circulating in the same direction as the J/ψ momentum is chosen (GJ forward), the resulting $\hat{z}$-axis is nearly collinear with the $\hat{z}$-axis of the HX and CS frames and points in the same direction. In GJ backward frame (beam circulating in the direction opposite to J/ψ momentum is chosen) the $\hat{z}$-axis points in the opposite direction.

While the angular decay coefficients depend heavily on the reference frame, it was noted in [12] that the λ_θ coefficient from various measurements transformed into the CS frames changes smoothly from longitudinal (negative) to transverse (positive) with increasing J/ψ momentum. The smooth variation occurs between measurements from fixed targets by E866/NuSea [13] and HERA-B [14], as well as a collider environment by CDF [15]. The transformation of the measurements depends on the assumption that the $\hat{z}$-axis of the CS frame is the natural frame, along which the J/ψ spin-alignment is purely longitudinal or transverse. The assumption is based on measurements of the angular distribution for inclusive J/ψ decays from fixed target $p+N$ collisions at HERA-B covering $p_T < 5$ GeV/c and $-0.3 < x_F < 0.1$ [14]. It has been predicted that the natural frame at large p_T is near to but not identically along the CS $\hat{z}$-axis [16]. Subsequent work reported in [17] obtained equations which could convert the angular parameters measured in one frame to another frame rotated around the $\hat{y}$-axis. A combination of polar and azimuthal constants can be arranged to form a frame-invariant angular decay coefficient

$$\tilde{\lambda} = \frac{\lambda_\theta + 3\lambda_\phi}{1 - \lambda_\phi}. \tag{4}$$

$\tilde{\lambda}$ is sensitive to the maximum angular asymmetry, or polarization, independent of the $\hat{z}$-axis orientation of the reference frame. A comparison between $\tilde{\lambda}$ derived from the azimuthal coefficients measured in the different reference frames can be used as a consistency check of the parameters extracted from the various reference frames.

While there is no clear prediction for the J/ψ spin-alignment from the CEM, it has been suggested that multiple soft gluon exchanges destroy the spin-alignment of the $c\bar{c}$ pair [18]. Recent calculations at NLO [6,7] and NNLO [8] in the CSM improve agreement with the spin-alignment measured previously at PHENIX [19], which is predicted at NLO to be longitudinal in the HX frame for large p_T [20]. Numerical estimates [21,22] in the NRQCD approach and recent calculations at NLO [23] predict a transverse spin-alignment in the HX frame at $p_T \gg M_{J/\psi}$ due to gluon fragmentation, which disagrees in both sign and magnitude with data from CDF [15]. Measurements of the J/ψ spin alignment in different kinematic regions can help distinguish the dominant production mechanism.

The PHENIX experiment has already published [19] a λ_θ measurement for J/ψ 's produced in $p+p$ collisions at $\sqrt{s} = 200$ GeV at midrapidity. In this paper we present a more comprehensive measurement of the full angular distributions for the leptonic decays of inclusive J/ψ in $p+p$ collisions at $\sqrt{s} = 510$ GeV for the HX, CS, GJ forward, and GJ backward reference frames. The measurement covers a transverse momentum range $2 < p_T < 10$ GeV/c and rapidity range $1.2 < y < 2.2$.

The experimental apparatus used to measure dimuon pairs from J/ψ decays is described in Sec. II. The procedure followed to obtain angular decay coefficients and their uncertainties is explained in Sec. III. The results, their comparison to other measurements and theoretical predictions are presented in Sec. IV.

II. EXPERIMENTAL SETUP AND J/ψ SELECTION

The measurements were carried out using the PHENIX detector [24] with data from $p+p$ collisions at $\sqrt{s} = 510$ GeV recorded in 2013. Decays of $J/\psi \to \mu^+\mu^-$ were measured in the muon spectrometer [25] for $1.2 < y < 2.2$ and full azimuthal angle. Collisions are identified by triggering on a minimal multiplicity of hits in two beam-beam counters (BBC) [26] placed at $3.0 < |\eta| < 3.9$. The data presented correspond to an integrated luminosity of 222 pb^{-1}. Approximately $117 \times 10^3 J/\psi$ mesons are used to determine the decay coefficients.

The PHENIX muon spectrometer comprises three finely-segmented multiplane cathode strip tracking chambers (MuTr) located in a radial magnetic field and positioned in front of five layers of Iarocci tubes interleaved with thick steel absorbers (MuID), which provide a hadron rejection of 10^{-4}. Events containing J/ψ mesons are triggered using logical units composed of all tubes in a window projecting from the vertex through the MuID. To satisfy the trigger, trigger logic units in the horizontal and vertical projection must contain at least one hit in either the first or second layer of the MuID, one

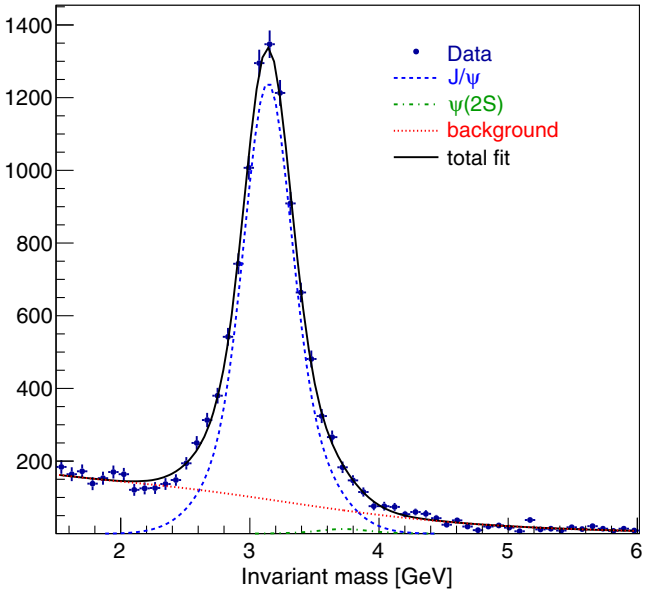

FIG. 2. An example of the invariant mass distribution of oppositely charged dimuon pairs after like-sign background subtraction (dark blue points) fit with a double Gaussian for the J/ψ (dashed blue curve) and $\psi(2S)$ (green dash-dotted curve) signals plus exponential for the background (dotted red curve). The solid black curve is the sum of signal and background fit.

additional hit in either the fourth or fifth layer, and at least three hits in total. To avoid the low-momentum region where the trigger efficiency changes quickly before reaching a plateau, the muons used in this analysis are required to have momentum along the beam direction $p_z > 1.45$ GeV/c as measured at the first MuTr station for the spectrometer, corresponding to ~2.1 GeV/c at the vertex.

Events are required to occur within 30 cm of the center of the experimental apparatus along the beam direction as measured by the beam-beam counters. To improve hadron rejection, a fit of the two tracks to the collision vertex was performed and required to have $\chi^2 < 5$ per degree of freedom. MuTr tracks and MuID hit roads were required to match within four standard deviations to ensure that they correspond to the same particle.

III. ANALYSIS PROCEDURE

In this section, we outline the procedure used to tune the simulation to data and extract both the shape of the J/ψ yield and the angular decay coefficients.

A. J/ψ reconstruction

The J/ψ mesons are reconstructed by calculating the invariant mass of all unlike-sign muon pairs after analysis cuts. Combinatorial random background is estimated by like-sign dimuons calculated as $2\sqrt{N^{++}N^{--}}$, where N^{++} and N^{--} are number of positive and negative same-sign pairs respectively, and subtracted. Mass distributions for each bin in p_T and rapidity are then fit using a double Gaussian as signal and exponential background to remove

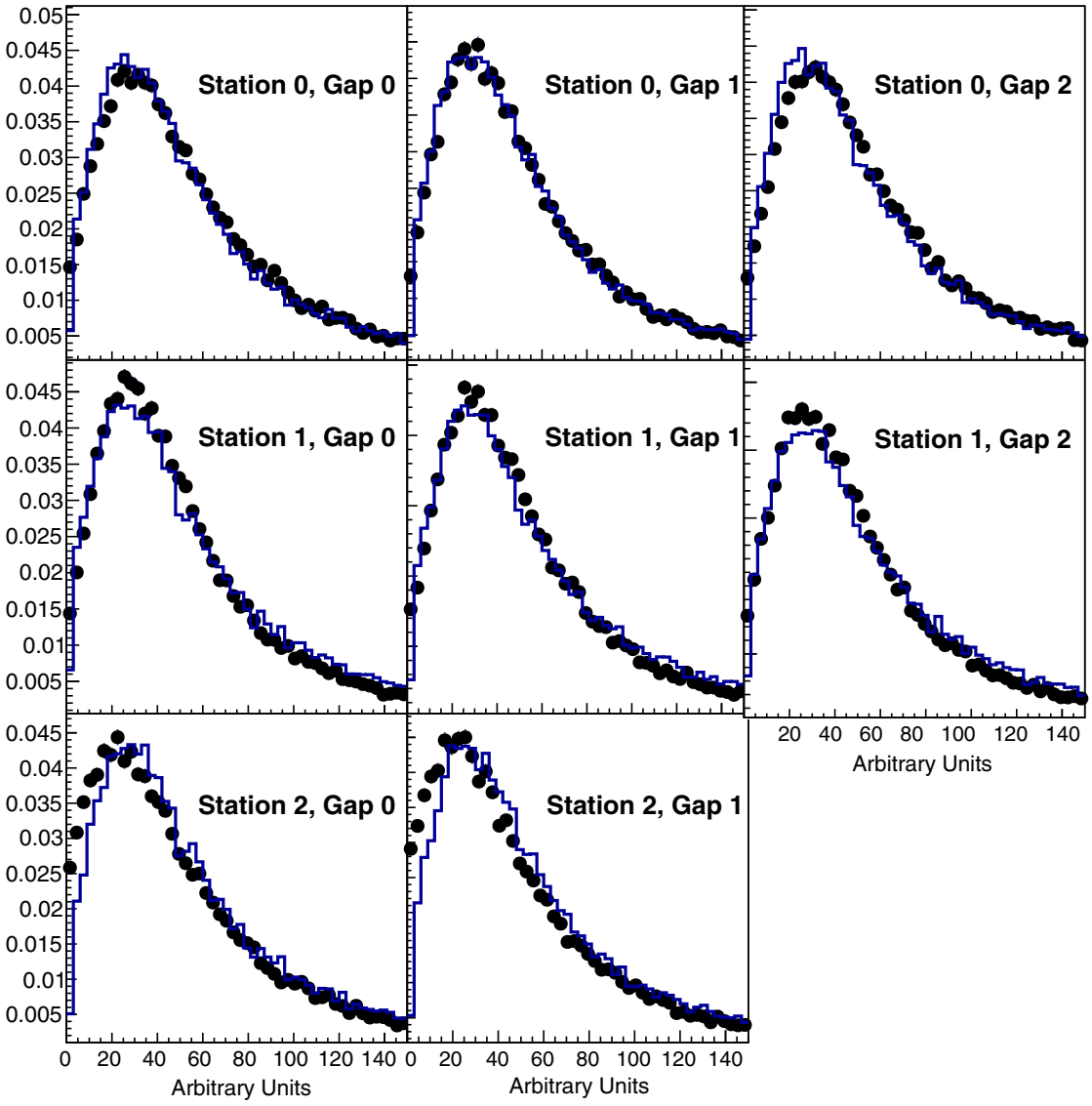

FIG. 3. A comparison of the total cluster charge distributions in the MuTr in simulation (blue histogram) and data (closed black circles). Each MuTr station is composed of three (Stations 1 and 2) or two (Station 3) measurement planes ("gaps") [25]. A cluster is the collection of ionization energy from the passage of a charged particle in the measurement plane.

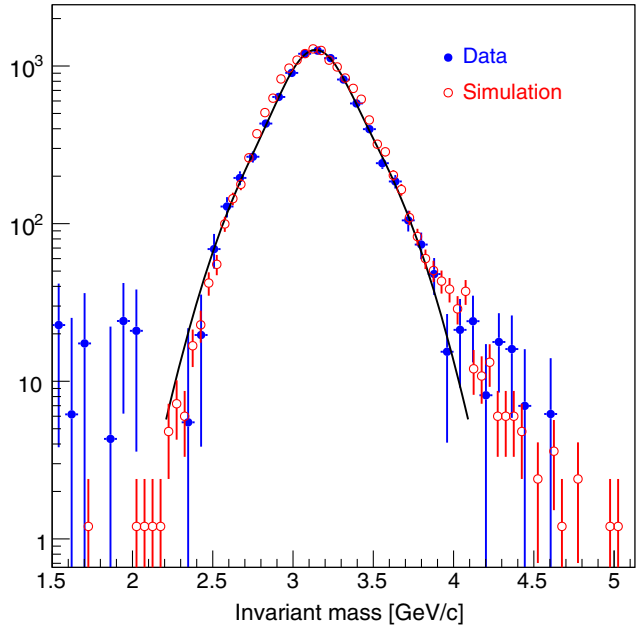

FIG. 4. Invariant mass distribution of simulated J/ψ (red open circles), and J/ψ 's reconstructed in data (solid blue dots) after all backgrounds are subtracted. The insert at the bottom shows (data-simulation)/σ difference, where σ is the statistical uncertainty of the difference.

dimuons from Drell-Yan and correlated open-heavy flavor decays (see Fig. 2). The number of J/ψ 's is obtained directly by integrating the dimuon invariant mass distribution in a mass interval from 2.5 to 3.7 GeV/c^2 after background subtraction. Background subtraction was performed for each individual $\cos\theta$-ϕ bin (see Sec. III C).

B. Experimental acceptance and simulation tuning

A simulation of J/ψ mesons generated by tuned PYTHIA 6.421 [27] is performed to determine the effects of the detector acceptance. As a complete GEANT 3 [28] model of the detector is used to obtain the efficiency and acceptance corrections in this analysis, the simulation itself needs to be well tuned to reproduce both low-level detector-related quantities and high level kinematic distributions. In particular, because we perform a two-dimensional fit to the data in $\cos\theta$-ϕ space for each reference frame, the inefficiencies in the experimental acceptance must be properly represented.

To ensure that the acceptance is approximately constant throughout the data-taking period, we excluded from analysis the data taken during time intervals when the MuTr or MuID had additional tripped high voltage channels over normal operation, or there were problems with data transmission from the detectors for $> 1\%$ of all events. Areas of the detectors that were disabled or highly inefficient are eliminated in both the analyzed data and simulations. In addition, for the MuTr, the charges deposited in individual strips within a MuTr cluster are smeared in the simulation to match the measured properties in the data.

An example of the excellent agreement between tuned simulations and data for the MuTr is shown in Fig. 3, where cluster charge distributions in data and simulation are compared. In addition to the low-level performance of the MuTr, the MuID detector has an efficiency for pairs of Iarocci tubes that is a function of the collision rate seen by the BBC, varying between 0.93 at 400 kHz to 0.88 at 2.2 MHz. The mean efficiency over the course of the running period is used as the efficiency of each pair, as a uniform change in efficiency will not affect the relative angular acceptance.

At a higher level, a good match of simulation to the data is demonstrated in Fig. 4, where the mass resolution for simulated and reconstructed J/ψ 's is compared.

Single unpolarized J/ψ 's were generated by PYTHIA and processed through full GEANT simulation. Even after the tuning described at the beginning of this chapter, small additional p_T and rapidity weights were still required to match the J/ψ 's p_T and rapidity distributions in PYTHIA to those measured experimentally. A systematic uncertainty, correlated between data points, was introduced to account for a possible mismatch between the p_T and rapidity distributions in simulation and data. This systematic uncertainty was estimated by varying the p_T and rapidity weights in simulation by 10%, or one standard deviation of the fits to the data (see Sec. III D for details). Because the detector acceptance in the simulation is sensitive to the input asymmetry in the decay muon distributions, the final step in the simulation was to apply angular decay coefficients obtained in the initial iteration as weights in the simulation, thus imitating the observed J/ψ polarization.

The relative acceptance as a function of p_T for the different reference frames is shown in Fig. 5.

C. Angular decay coefficients

To extract the angular decay coefficients, the background subtracted J/ψ yields are histogrammed according to the angular distribution of the positive muon in twelve bins of $\cos\theta$ by ten bins of ϕ, and three bins in p_T (2–3, 3–4, and 4–10 GeV/c) for each reference frame. The mean p_T for each bin are 2.47, 3.46, and 5.45 GeV/c, respectively. The experimental data are corrected for acceptance, and then fit with Eq. (3). The fit is performed simultaneously in $\cos\theta$ and ϕ to extract all three angular decay coefficients λ_θ, $\lambda_{\theta\phi}$, λ_ϕ, and frame-independent $\tilde{\lambda}$. In general the fits to the data are good, with a typical χ^2 value per degree of freedom between 1.2–2.1, with the number of degrees of freedom typically in the 40–60 range.

The exact fitting procedure is outlined below.

(1) The J/ψ angular distributions are divided into 12 bins in $\cos\theta$ and 10 bins in ϕ. Combinatorial and correlated background is subtracted bin-by-bin, and angular distributions are then corrected for acceptance, which is calculated assuming no polarization, that is $\lambda_\theta = \lambda_{\theta\phi} = \lambda_\phi = 0$. This is done for each of the three transverse momentum bins in each polarization frame.

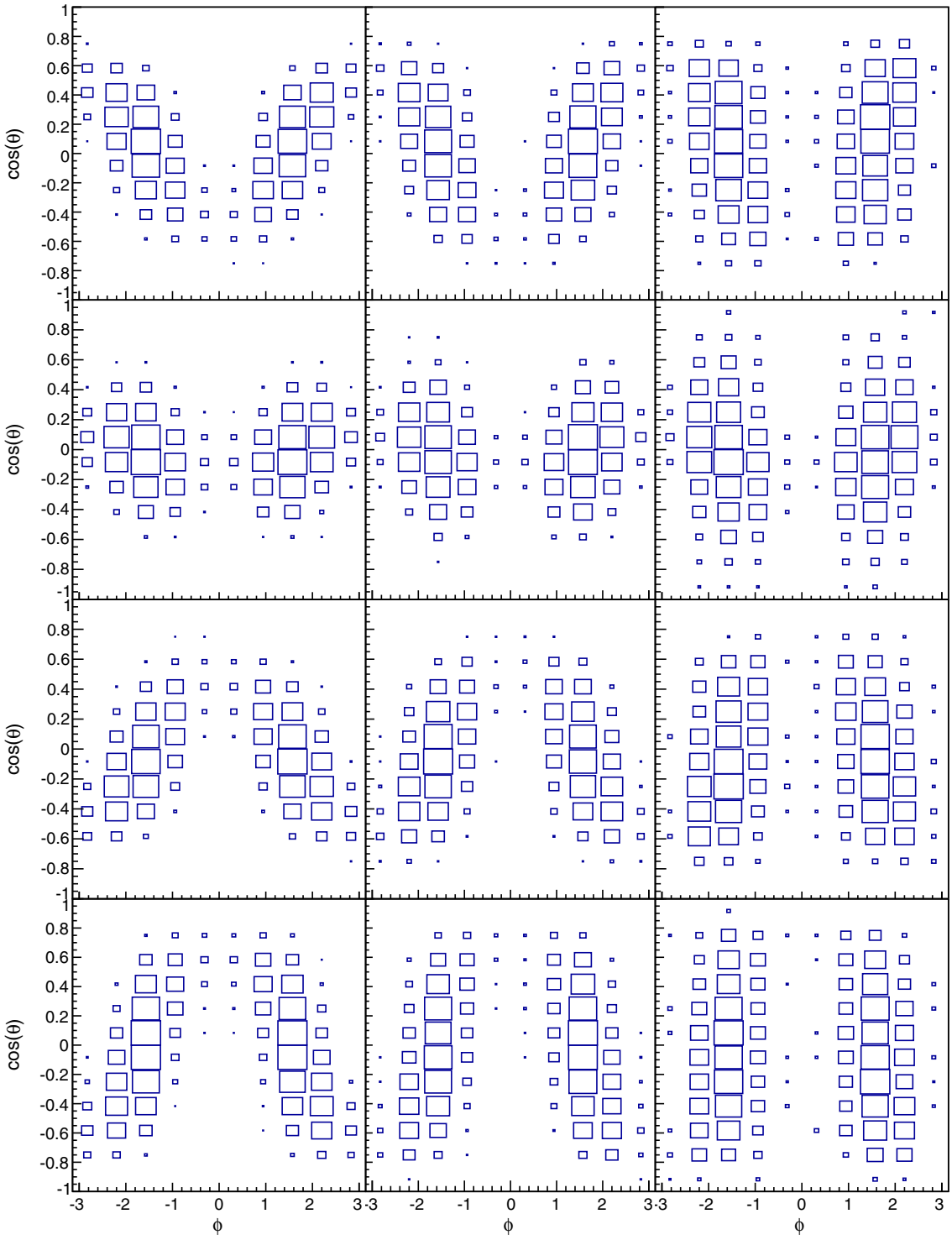

FIG. 5. Relative acceptance in $\cos\theta$-ϕ bins in (from top to bottom) the HX, CS, GJ Backward, and GJ Forward frames for increasing p_T from left to right. The area of rectangles is proportional to acceptance value in linear scale. See Sec. III C for definition of p_T, $\cos\theta$, and ϕ bins.

(2) λ_θ, $\lambda_{\theta\phi}$, and λ_ϕ in Eq. (3) are varied separately and independently from -1 to 1 with a 0.01 step, and for each step a fit is done to the acceptance corrected measured angular distribution. The fit is done for a fixed value of all λ's. The only free parameter is absolute normalization. A χ^2 of the fit is calculated at each step. The minimum χ^2 obtained in the three dimensional phase space spanned by λ_θ, $\lambda_{\theta\phi}$ and λ_ϕ is chosen as the best fit.

(3) Extracted λ coefficients are used as weights in the simulation to generate acceptance for polarized J/ψ which is used in the next iteration. Convergence is achieved when the newly extracted λ coefficients become zero within the experimental uncertainty, which means that the polarization in the simulation matches that in the data.

The resulting angular decay coefficients λ_θ, $\lambda_{\theta\phi}$, λ_ϕ, and frame-independent coefficient $\tilde{\lambda}$ are shown in Fig. 6, Fig. 7, Fig. 8, and Fig. 9 respectively, for four reference frames as a function of transverse momentum.

D. Systematic uncertainty discussion

The statistical uncertainties of the angular decay coefficients were calculated by randomizing each bin in $\cos\theta$ vs. ϕ histograms with a Gaussian random number according to the statistical uncertainty in that bin, and refitting. This procedure was repeated one hundred times, and the RMS of the resulting λ distribution was taken as a statistical uncertainty.

A measurement of the angular decay coefficients is sensitive to several factors, including the input p_T and rapidity distribution in the simulation, exact matching of acceptance between data and simulation, how well the simulation reproduces low-level detector-related quantities, and time-varying conditions. These uncertainties were estimated by introducing variations in the input p_T and rapidity distributions, fiducial cuts, and low-level deposited charge smearing in the simulation. Additional cross-checks included variations of the collision vertex cut and J/ψ rapidity cut. Possible polarization bias in acceptance was studied with a simulation-based blind analysis. In this blind

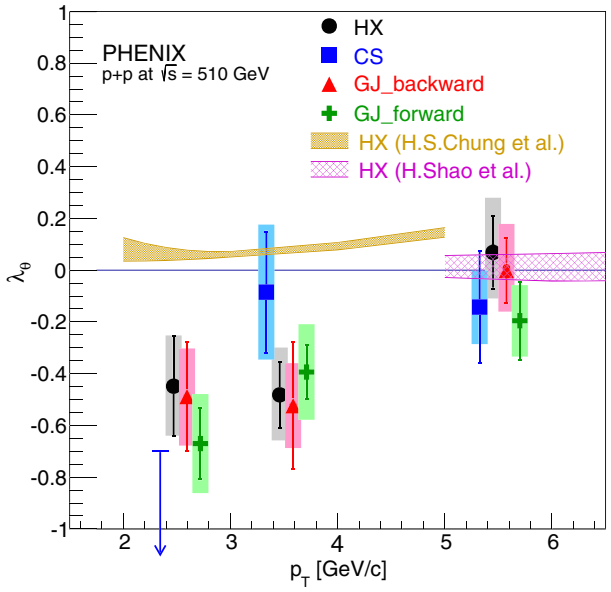

FIG. 6. Polar angular decay coefficient λ_θ as a function of transverse momentum for four reference frames and three p_T bins. Black circles: HX frame; blue squares: CS frame; red triangles: GJ Backward; green crosses: GJ Forward frames. Shaded error boxes show systematic uncertainty. Points are shifted in p_T for clarity. Down-pointing arrow indicates 90% confidence level upper limit. The data are compared with NRQCD theoretical predictions in Helicity frame by H. S. Chung *et al.* [29] and H. Shao *et al.* [30].

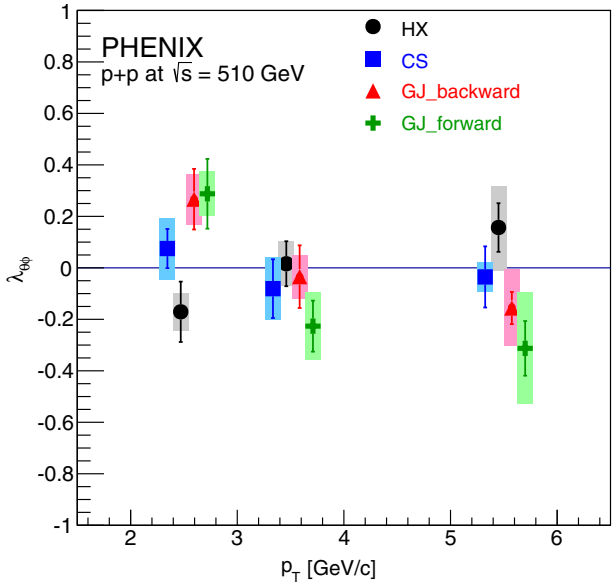

FIG. 7. "Mixed" angular decay coefficient $\lambda_{\theta\phi}$ as a function of transverse momentum for four reference frames and three p_T bins. Black circles: HX frame; blue squares: CS frame; red triangles: GJ Backward; green crosses: GJ Forward frames. Shaded error boxes show systematic uncertainty. Points are shifted in p_T for clarity.

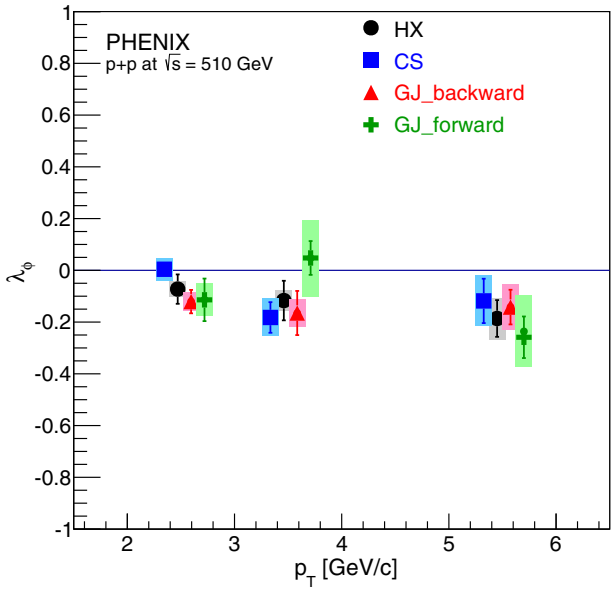

FIG. 8. Azimuthal angular decay coefficient λ_ϕ as a function of transverse momentum for four reference frames and three p_T bins. Black circles: HX frame; blue squares: CS frame; red triangles: GJ Backward; green crosses: GJ Forward frames. Shaded error boxes show systematic uncertainty. Points are shifted in p_T for clarity.

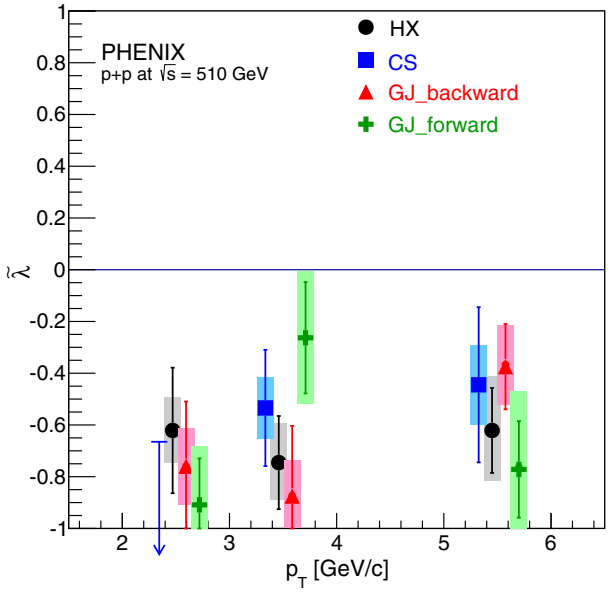

FIG. 9. Frame-independent angular decay coefficient $\tilde{\lambda}$ as a function of transverse momentum for the four reference frames and three p_T bins. Black circles: HX frame; blue squares: CS frame; red triangles: GJ Backward; green crosses: GJ Forward frames. Shaded error boxes show systematic uncertainty. Points are shifted in p_T for clarity. Down pointing arrow indicates 90% confidence level upper limit.

analysis simulated J/ψ 's generated with a certain polarization were used as fake data. A full analysis of the fake data was performed without prior knowledge of the input polarization, polarization coefficients were extracted and compared to the input values.

The resulting variations in angular decay coefficients were accounted for as systematic uncertainties and are listed in Table I.

The total systematic uncertainty shown as shaded boxes in Figs. 6 through 9 is taken to be the quadratic sum of these components, assuming that they are uncorrelated.

IV. RESULTS AND DISCUSSION

We have presented the first measurement of the full angular distribution from J/ψ decays to muons in $p+p$ collisions at $\sqrt{s}=510$ GeV at forward rapidity $(1.2<y<2.2)$ in the Helicity, Collins-Soper, and Gottfried-Jackson reference frames. The results are summarized in Tables II and III, and in Figs. 6 through 9.

The measurements presented here are for inclusive J/ψ. Feed-down from higher mass quarkonium states also contribute to the observed polarization and is not separated out.

In all frames the polar coefficient λ_θ is strongly negative at low p_T and becomes close to zero at high p_T, while the azimuthal coefficient λ_ϕ is close to zero at low p_T, and becomes slightly negative at higher p_T.

TABLE I. Systematic uncertainties in the polarization measurement.

		λ_θ			$\tilde{\lambda}$			λ_ϕ			$\lambda_{\theta\phi}$		
p_T bin [GeV/c]:		2–3	3–4	4–10	2–3	3–4	4–10	2–3	3–4	4–10	2–3	3–4	4–10
HX	Acceptance	0.134	0.118	0.103	0.082	0.082	0.075	0.010	0.024	0.034	0.052	0.077	0.076
	Kinematics	$^{+0.049}_{-0.023}$	$^{+0.050}_{-0.008}$	$^{+0.120}_{-0.038}$	$^{+0.036}_{-0.004}$	$^{+0.042}_{-0.001}$	$^{+0.089}_{-0.049}$	$^{+0.006}_{-0.009}$	$^{+0.002}_{-0.004}$	$^{+0.021}_{-0.028}$	$^{+0.003}_{-0.012}$	$^{+0.014}_{-0.010}$	$^{+0.012}_{-0.043}$
	Hit smearing	0.134	0.131	0.140	0.094	0.119	0.173	0.027	0.031	0.067	0.050	0.035	0.142
	Polarization bias	0.015	0.010	0.005	0.016	0.011	0.006	0.002	0.002	0.001	0.010	0.008	0.005
	TOTAL	$^{+0.196}_{-0.191}$	$^{+0.183}_{-0.176}$	$^{+0.211}_{-0.178}$	$^{+0.130}_{-0.125}$	$^{+0.150}_{-0.144}$	$^{+0.209}_{-0.195}$	$^{+0.030}_{-0.031}$	$^{+0.039}_{-0.039}$	$^{+0.079}_{-0.081}$	$^{+0.072}_{-0.073}$	$^{+0.086}_{-0.085}$	$^{+0.162}_{-0.167}$
CS	Acceptance	0.106	0.148	0.079	0.076	0.101	0.083	0.010	0.010	0.025	0.061	0.076	0.042
	Kinematics	$^{+0.011}_{-0.004}$	$^{+0.020}_{-0.014}$	$^{+0.061}_{-0.066}$	$^{+0.0147}_{-0.006}$	$^{+0.014}_{-0.016}$	$^{+0.068}_{-0.074}$	$^{+0.003}_{-0.001}$	$^{+0.001}_{-0.004}$	$^{+0.020}_{-0.020}$	$^{+0.016}_{-0.015}$	$^{+0.011}_{-0.025}$	$^{+0.019}_{-0.025}$
	Hit smearing	0.085	0.214	0.099	0.045	0.061	0.107	0.042	0.072	0.092	0.102	0.092	0.032
	Polarization bias	0.016	0.012	0.006	0.017	0.013	0.007	0.002	0.002	0.0015	0.011	0.009	0.007
	TOTAL	$^{+0.136}_{-0.136}$	$^{+0.261}_{-0.261}$	$^{+0.141}_{-0.143}$	$^{+0.089}_{-0.088}$	$^{+0.118}_{-0.119}$	$^{+0.151}_{-0.154}$	$^{+0.043}_{-0.043}$	$^{+0.073}_{-0.073}$	$^{+0.098}_{-0.098}$	$^{+0.120}_{-0.120}$	$^{+0.120}_{-0.122}$	$^{+0.057}_{-0.059}$
GJB	Acceptance	0.111	0.138	0.081	0.086	0.106	0.089	0.012	0.013	0.026	0.065	0.071	0.045
	Kinematics	$^{+0.013}_{-0.037}$	$^{+0.021}_{-0.003}$	$^{+0.106}_{-0.064}$	$^{+0.005}_{-0.018}$	$^{+0.029}_{-0.019}$	$^{+0.075}_{-0.033}$	$^{+0.010}_{-0.009}$	$^{+0.007}_{-0.015}$	$^{+0.013}_{-0.005}$	$^{+0.013}_{-0.008}$	$^{+0.013}_{-0.019}$	$^{+0.054}_{-0.037}$
	Hit smearing	0.149	0.087	0.121	0.119	0.082	0.112	0.032	0.050	0.083	0.074	0.041	0.133
	Polarization bias	0.018	0.009	0.004	0.019	0.010	0.005	0.002	0.002	0.002	0.016	0.009	0.005
	TOTAL	$^{+0.186}_{-0.189}$	$^{+0.165}_{-0.163}$	$^{+0.180}_{-0.159}$	$^{+0.147}_{-0.148}$	$^{+0.137}_{-0.136}$	$^{+0.162}_{-0.147}$	$^{+0.035}_{-0.035}$	$^{+0.052}_{-0.054}$	$^{+0.088}_{-0.087}$	$^{+0.099}_{-0.098}$	$^{+0.083}_{-0.084}$	$^{+0.151}_{-0.145}$
GJF	Acceptance	0.129	0.122	0.120	0.081	0.084	0.078	0.015	0.026	0.035	0.061	0.076	0.074
	Kinematics	$^{+0.005}_{-0.000}$	$^{+0.024}_{-0.020}$	$^{+0.008}_{-0.020}$	$^{+0.029}_{-0.019}$	$^{+0.007}_{-0.006}$	$^{+0.096}_{-0.013}$	$^{+0.017}_{-0.009}$	$^{+0.006}_{-0.016}$	$^{+0.112}_{-0.002}$	$^{+0.022}_{-0.016}$	$^{+0.023}_{-0.000}$	$^{+0.044}_{-0.026}$
	Hit smearing	0.141	0.137	0.067	0.212	0.243	0.276	0.060	0.145	0.110	0.058	0.106	0.200
	Polarization bias	0.015	0.012	0.006	0.016	0.013	0.007	0.002	0.001	0.001	0.013	0.010	0.007
	TOTAL	$^{+0.192}_{-0.191}$	$^{+0.185}_{-0.184}$	$^{+0.137}_{-0.139}$	$^{+0.229}_{-0.227}$	$^{+0.257}_{-0.257}$	$^{+0.303}_{-0.287}$	$^{+0.064}_{-0.063}$	$^{+0.148}_{-0.149}$	$^{+0.160}_{-0.115}$	$^{+0.087}_{-0.086}$	$^{+0.133}_{-0.131}$	$^{+0.217}_{-0.214}$

TABLE II. λ_θ and $\tilde{\lambda}$ in four frames. Only statistical errors are shown. Mean p_T for each of the three bins are 2.47, 3.46, and 5.45 GeV/c respectively. The numbers in the CS frame for the $p_T = 2$–3 GeV/c bin are 90% confidence level upper limits.

	λ_θ			$\tilde{\lambda}$		
p_T bin [GeV/c]:	2–3	3–4	4–10	2–3	3–4	4–10
HX	-0.449 ± 0.195	-0.482 ± 0.131	0.069 ± 0.142	-0.621 ± 0.241	-0.745 ± 0.180	-0.621 ± 0.163
CS	< -0.701	-0.085 ± 0.238	-0.143 ± 0.221	< -0.665	-0.534 ± 0.221	-0.445 ± 0.305
GJB	-0.489 ± 0.218	-0.524 ± 0.252	-0.002 ± 0.134	-0.760 ± 0.256	-0.875 ± 0.279	-0.375 ± 0.171
GJF	-0.670 ± 0.141	-0.394 ± 0.105	-0.195 ± 0.151	-0.909 ± 0.185	-0.263 ± 0.221	-0.772 ± 0.190

TABLE III. λ_ϕ and $\lambda_{\theta\phi}$ in four frames. Only statistical errors are shown. Mean p_T for each of the three bins are 2.47, 3.46, and 5.45 GeV/c respectively.

	λ_ϕ			$\lambda_{\theta\phi}$		
p_T bin [GeV/c]:	2–3	3–4	4–10	2–3	3–4	4–10
HX	-0.073 ± 0.057	-0.117 ± 0.077	-0.186 ± 0.071	-0.171 ± 0.120	0.016 ± 0.087	0.157 ± 0.094
CS	0.004 ± 0.027	-0.182 ± 0.059	-0.118 ± 0.086	0.075 ± 0.076	-0.081 ± 0.110	-0.035 ± 0.120
GJB	-0.121 ± 0.045	-0.165 ± 0.085	-0.142 ± 0.067	0.267 ± 0.120	-0.034 ± 0.120	-0.156 ± 0.063
GJF	-0.114 ± 0.082	0.048 ± 0.065	-0.259 ± 0.080	0.288 ± 0.140	-0.230 ± 0.100	-0.313 ± 0.110

The frame-independent coefficient $\tilde{\lambda}$ is strongly negative at all p_T in all frames. Consistency of $\tilde{\lambda}$ values in all polarization frames indicates that systematic uncertainties are well under control. The obtained polarization coefficient $\tilde{\lambda}$ is in good agreement with what was reported by the STAR experiment [31], for the same $\sqrt{s}$ at midrapidity and higher transverse momentum.

At the Large Hadron Collider (LHC), the LHCb experiment [32] reported similar, although smaller values of λ_θ with similar trend in transverse momentum at forward rapidity. λ_θ measured by the ALICE experiment [33] at forward rapidity is consistent with no polarization, although, within experimental uncertainty, it can be said to be similar to the LHCb result. A very comprehensive CMS measurement [34] indicates that both λ_θ and $\tilde{\lambda}$ are consistent with zero. However, note that the CMS measurement covers much a higher transverse momentum range and for more central rapidities.

The measured polar coefficient λ_θ is compared to theoretical prediction for prompt J/ψ in Helicity frame calculated in the NRQCD factorization approach by H. S. Chung *et al.* [29] and H. Shao [30] in Fig. 6. At high transverse momentum both predictions are in good agreement with the data, while at low p_T a strong deviation can be seen. While theory expects λ_θ to be small and slightly positive at low p_T, it is strongly negative in the data. The polar coefficient result in the Helicity frame poses a challenge to the NRQCD effective theory at low p_T, where perturbative calculations are more difficult to compute. No theoretical calculation is available for the frame-independent coefficient $\tilde{\lambda}$ or for other reference frames. The reported experimental results represent a challenge for the theory and provide a basis for better understanding of quarkonium production in high energy $p + p$ collisions.

ACKNOWLEDGMENTS

We thank the staff of the Collider-Accelerator and Physics Departments at Brookhaven National Laboratory and the staff of the other PHENIX participating institutions for their vital contributions. We acknowledge support from the Office of Nuclear Physics in the Office of Science of the Department of Energy, the National Science Foundation, Abilene Christian University Research Council, Research Foundation of SUNY, and Dean of the College of Arts and Sciences, Vanderbilt University (U.S.A), Ministry of Education, Culture, Sports, Science, and Technology and the Japan Society for the Promotion of Science (Japan), Conselho Nacional de Desenvolvimento Científico e Tecnológico and Fundação de Amparo à Pesquisa do Estado de São Paulo (Brazil), Natural Science Foundation of China (People's Republic of China), Croatian Science Foundation and Ministry of Science and Education (Croatia), Ministry of Education, Youth and Sports (Czech Republic), Centre National de la Recherche Scientifique, Commissariat à l'Énergie Atomique, and Institut National de Physique Nucléaire et de Physique des Particules (France), Bundesministerium für Bildung und Forschung, Deutscher Akademischer Austausch Dienst, and Alexander von Humboldt Stiftung (Germany), National Science Fund, OTKA, EFOP, and the Ch. Simonyi Fund (Hungary), Department of Atomic Energy and Department of Science and Technology (India), Israel Science Foundation (Israel), Basic

Science Research Program through NRF of the Ministry of Education (Korea), Physics Department, Lahore University of Management Sciences (Pakistan), Ministry of Education and Science, Russian Academy of Sciences, Federal Agency of Atomic Energy (Russia), VR and Wallenberg Foundation (Sweden), the U.S. Civilian Research and Development Foundation for the Independent States of the Former Soviet Union, the Hungarian American Enterprise Scholarship Fund, and the US-Israel Binational Science Foundation.

[1] G. T. Bodwin, E. Braaten, and G. P. Lepage, Rigorous QCD analysis of inclusive annihilation and production of heavy quarkonium, Phys. Rev. D **51**, 1125 (1995).
[2] H. Fritzsch, Producing heavy quark flavors in hadronic collisions: A test of quantum chromodynamics, Phys. Lett. B **67B**, 217 (1977).
[3] R. Baier and R. Ruckl, Hadronic production of J/ψ and Υ: Transverse momentum distributions, Phys. Lett. B **102B**, 364 (1981).
[4] F. Abe *et al.* (CDF Collaboration), J/ψ and $\psi(2S)$ Production in $p\bar{p}$ Collisions at $\sqrt{s} = 1.8$ TeV, Phys. Rev. Lett. **79**, 572 (1997).
[5] A. Adare *et al.* (PHENIX Collaboration), J/ψ Production Versus Transverse Momentum and Rapidity in p^+p Collisions at $\sqrt{s} = 200$-GeV, Phys. Rev. Lett. **98**, 232002 (2007).
[6] P. Artoisenet, J. M. Campbell, F. Maltoni, and F. Tramontano, J/ψ Production at HERA, Phys. Rev. Lett. **102**, 142001 (2009).
[7] C.-H. Chang, R. Li, and J.-X. Wang, J/ψ polarization in photo-production up-to the next-to- leading order of QCD, Phys. Rev. D **80**, 034020 (2009).
[8] P. Artoisenet, J. M. Campbell, J. P. Lansberg, F. Maltoni, and F. Tramontano, υ Production at Fermilab Tevatron and LHC Energies, Phys. Rev. Lett. **101**, 152001 (2008).
[9] M. Jacob and G. C. Wick, On the general theory of collisions for particles with spin, Ann. Phys. (N.Y.) **7**, 404 (1959).
[10] J. C. Collins and D. E. Soper, Angular distribution of dileptons in high-energy hadron collisions, Phys. Rev. D **16**, 2219 (1977).
[11] K. Gottfried and J. D. Jackson, On the connection between production mechanism and decay of resonances at high energies, Nuovo Cimento **33**, 309 (1964).
[12] P. Faccioli, C. Lourenco, J. Seixas, and H. K. Wohri, J/ψ Polarization from Fixed-Target to Collider Energies, Phys. Rev. Lett. **102**, 151802 (2009).
[13] T. H. Chang *et al.* (FNAL E866/NuSea Collaboration), J/ψ Polarization in 800-GeV p Cu Interactions, Phys. Rev. Lett. **91**, 211801 (2003).
[14] I. Abt *et al.* (HERA-B Collaboration), Angular distributions of leptons from J/ψ s produced in 920 GeV fixed-target proton-nucleus collisions, Eur. Phys. J. C **60**, 517 (2009).
[15] A. Abulencia *et al.* (CDF Collaboration), Polarization of J/ψ and $\psi(2S)$ Mesons Produced in $p + \bar{p}$ Collisions at $\sqrt{s} = 1.96$-TeV, Phys. Rev. Lett. **99**, 132001 (2007).
[16] E. Braaten, D. Kang, J. Lee, and C. Yu, Optimal spin quantization axes for quarkonium with large transverse momentum, Phys. Rev. D **79**, 054013 (2009).
[17] P. Faccioli, C. Lourenco, J. Seixas, and H. K. Wohri, Towards the experimental clarification of quarkonium polarization, Eur. Phys. J. C **69**, 657 (2010).
[18] J. F. Amundson, Oscar J. P. Eboli, E. M. Gregores, and F. Halzen, Quantitative tests of color evaporation: Charmonium production, Phys. Lett. B **390**, 323 (1997).
[19] A. Adare *et al.* (PHENIX Collaboration), Transverse momentum dependence of J/ψ polarization at midrapidity in p + p collisions at sqrt(s) = 200 GeV, Phys. Rev. D **82**, 012001 (2010).
[20] J. P. Lansberg, QCD corrections to J/ψ polarisation in pp collisions at RHIC, Phys. Lett. B **695**, 149 (2011).
[21] M. Beneke and M. Kramer, Direct J/ψ and ψ' polarization and cross- sections at the Tevatron, Phys. Rev. D **55**, R5269 (1997).
[22] E. Braaten, B. A. Kniehl, and J. Lee, Polarization of prompt J/ψ at the Tevatron, Phys. Rev. D **62**, 094005 (2000).
[23] B. Gong, X. Q. Li, and J. X. Wang, QCD corrections to J/ψ production via color octet states at Tevatron and LHC, Phys. Lett. B **673**, 197 (2009).
[24] K. Adcox *et al.* (PHENIX Collaboration), PHENIX detector overview, Nucl. Instrum. Methods Phys. Res., Sect. A **499**, 469 (2003).
[25] H. Akikawa *et al.* (PHENIX Collaboration), PHENIX muon arms, Nucl. Instrum. Methods Phys. Res., Sect. A **499**, 537 (2003).
[26] M. Allen *et al.* (PHENIX Collaboration), Phenix inner detectors, Nucl. Instrum. Methods Phys. Res., Sect. A **499**, 549 (2003).
[27] T. Sjostrand, P. Eden, C. Friberg, L. Lonnblad, G. Miu, S. Mrenna, and E. Norrbin, High-energy physics event generation with PYTHIA 6.1, Comput. Phys. Commun. **135**, 238 (2001).
[28] GEANT 3.2.1, CERN Computing Library (1993), http://wwwasdoc.web.cern.ch/wwwasdoc/pdfdir/geant.pdf.
[29] H. S. Chung, S. Kim, J. Lee, and C. Yu, Polarization of prompt J/ψ in $pp \to J/\psi + \mathrm{X}$ at $\sqrt{s} = 200$ GeV, Phys. Rev. D **83**, 037501 (2011).
[30] H.-S. Shao, H. Han, Y.-Q. Ma, C. Meng, Y.-J. Zhang, and K.-T. Chao, Yields and polarizations of prompt J/ψ and $\psi(2S)$ production in hadronic collisions, J. High Energy Phys. 05 (2015) 103.

[31] B. Trzeciak (STAR Collaboration), J/ψ polarization measurements in p + p collisions at $\sqrt{s} = 200$ and 500 GeV with the STAR experiment, *Proc. Sci.*, EPS-HEP2015 (2015) 470.

[32] R Aaij *et al.* (LHCb Collaboration), Measurement of J/ψ polarization in pp collisions at $\sqrt{s} = 7$ TeV, Eur. Phys. J. C **73**, 2631 (2013).

[33] B. Abelev *et al.* (ALICE Collaboration), J/ψ Polarization in pp Collisions at $\sqrt{s} = 7$ TeV, Phys. Rev. Lett. **108**, 082001 (2012).

[34] S. Chatrchyan *et al.* (CMS Collaboration), Measurement of the prompt J/ψ and $\psi(2S)$ polarizations in pp collisions at $\sqrt{s} = 7$ TeV, Phys. Lett. B **727**, 381 (2013).